Original Article | Pediatric Imaging

eISSN 2005-8330
https://doi.org/10.3348/kjr.2020.0850
Korean J Radiol 2021;22(9):1525-1536

Korean Journal of Radiology
KJR

Feasibility of Three-Dimensional Balanced Steady-State Free Precession Cine Magnetic Resonance Imaging Combined with an Image Denoising Technique to Evaluate Cardiac Function in Children with Repaired Tetralogy of Fallot

YaFeng Peng[1]*, XinYu Su[2]*, LiWei Hu[1], Qian Wang[1], RongZhen Ouyang[1], AiMin Sun[1], Chen Guo[1], XiaoFen Yao[1], Yong Zhang[3], LiJia Wang[2], YuMin Zhong[1]

[1]Diagnostic Imaging Center of Shanghai Children's Medical Center Affiliated with Shanghai Jiao Tong University School of Medicine, Shanghai, China; [2]University of Shanghai for Science and Technology, Institute of Medical Imaging Engineering, School of Medical Instrument and Food Engineering, Shanghai, China; [3]MR Research, GE Healthcare, Shanghai, China

Objective: To investigate the feasibility of cine three-dimensional (3D) balanced steady-state free precession (b-SSFP) imaging combined with a non-local means (NLM) algorithm for image denoising in evaluating cardiac function in children with repaired tetralogy of Fallot (rTOF).

Materials and Methods: Thirty-five patients with rTOF (mean age, 12 years; range, 7–18 years) were enrolled to undergo cardiac cine image acquisition, including two-dimensional (2D) b-SSFP, 3D b-SSFP, and 3D b-SSFP combined with NLM. End-diastolic volume (EDV), end-systolic volume (ESV), stroke volume (SV), and ejection fraction (EF) of the two ventricles were measured and indexed by body surface index. Acquisition time and image quality were recorded and compared among the three imaging sequences.

Results: 3D b-SSFP with denoising vs. 2D b-SSFP had high correlation coefficients for EDV, ESV, SV, and EF of the left (0.959–0.991; $p < 0.001$) as well as right (0.755–0.965; $p < 0.001$) ventricular metrics. The image acquisition time ± standard deviation (SD) was 25.1 ± 2.4 seconds for 3D b-SSFP compared with 277.6 ± 0.7 seconds for 2D b-SSFP, indicating a significantly shorter time with the 3D than the 2D sequence ($p < 0.001$). Image quality score was better with 3D b-SSFP combined with denoising than with 3D b-SSFP (mean ± SD, 3.8 ± 0.6 vs. 3.5 ± 0.6; $p = 0.005$). Signal-to-noise ratios for blood and myocardium as well as contrast between blood and myocardium were higher for 3D b-SSFP combined with denoising than for 3D b-SSFP ($p < 0.05$ for all but septal myocardium).

Conclusion: The 3D b-SSFP sequence can significantly reduce acquisition time compared to the 2D b-SSFP sequence for cine imaging in the evaluation of ventricular function in children with rTOF, and its quality can be further improved by combining it with an NLM denoising method.

Keywords: *Congenital heart disease; Tetralogy of Fallot; Cardiac function; Pediatrics; Cine magnetic resonance imaging*

Received: July 3, 2020 **Revised:** March 6, 2021 **Accepted:** March 13, 2021

This work was supported by the National Key Research and Development Program of China (No.2018YFB110710), Shanghai Committee of Science and Technology (No.17411965400).

*These authors contributed equally to this work.

Corresponding author: YuMin Zhong, MD, PhD, Diagnostic Imaging Center of Shanghai Children's Medical Center Affiliated with Shanghai Jiao Tong University School of Medicine, No.1678 Dong Fang Road, Shanghai 200127, China.

• E-mail: zyumin2002@163.com

INTRODUCTION

Cardiac magnetic resonance (CMR) imaging is regarded as the gold standard for noninvasive assessment of cardiac morphology and function after surgery for congenital heart diseases (CHD) such as tetralogy of Fallot (TOF) [1]. Cine two-dimensional (2D) balanced steady-state free precession (b-SSFP) is a popular imaging method because it is relatively time-efficient and has good spatial resolution and high blood-to-myocardium contrast, especially at 1.5T [2,3]. Due to the long acquisition time of whole-heart CMR, it is difficult to encourage cooperation in young children; thus, sedation and anesthesia may be required. Fast acquisition technology can be used to circumvent this issue. A cine three-dimensional (3D) b-SSFP with a k-adaptive-t auto-calibrating reconstruction (kat ARC) for the Cartesian sampling acceleration method was used to reduce the acquisition time by approximately 20 times. With this method, whole-heart acquisition can be completed in one breath hold [4]. To acquire whole-heart data and evaluate cardiac function, multiple cardiac imaging planes have to be obtained using conventional cine 2D b-SSFP, while 3D images can be reformatted into multiple planes and the time required to acquire different planes of cardiac images can be saved. However, with whole-heart volumetric imaging acquisition, cine 3D b-SSFP intrinsically suffers from reduced in-flow blood enhancement; thus, its lower contrast is apparent between the myocardium and the blood pool when compared with cine 2D b-SSFP [5]. Image denoising techniques increase image contrast by removing image noise and retaining important features, such as the image contrast of cardiac edges and image texture [6]. The purpose of this study was to evaluate the feasibility of cine 3D b-SSFP combined with a non-local means (NLM) denoising method for assessing cardiac function in patients with repaired TOF (rTOF).

MATERIALS AND METHODS

This study was conducted according to the principles of the Declaration of Helsinki and was approved by the Institutional Ethics Committee (IRB No. SCMCIRB-K2016051). All patients (or their legal guardians) provided informed consent for participation.

Study Population

Thirty-five subjects with rTOF (mean age, 12 years; range, 7–18 years) were prospectively recruited from August 2018 to February 2019. The exclusion criteria were as follows: 1) contraindications to MRI scanning, 2) severe arrhythmia, or 3) claustrophobia. Demographic information was collected from each patient on the day of the CMR examination.

MRI Protocol

All imaging examinations were performed using a commercial 3T MRI scanner (MR750, GE Healthcare). All patients underwent cine 2D b-SSFP and cine 3D b-SSFP. Cine 2D b-SSFP was used to image the left and right ventricular outflow tracts in three-chamber, four-chamber, and short-axis views. The contrast agent used was gadodiamide

Table 1. Imaging Parameters of 2D Cine Sequences and 3D Cine Sequences

Parameters	2D Cine	3D Cine
TR, ms	3.3–3.6	2.8–3.2
TE, ms	1.6–1.8	1.1–1.3
Flip angle, °	45	45
FOV, mm	300 x 400	300 x 400
Matrix	160 x 160	192 x 212
Acquired voxel size, mm	1.8–2.5 x 1.8–2.5 x 6–8	1.6–2.1 x 1.4–1.9 x 6–8
Reconstructed voxel size, mm	1.1–1.5 x 1.1–1.5 x 6–8	1.1–1.5 x 1.1–1.5 x 6–8
Parallel acquisition acceleration factor	2	8–9
Temporal resolution, ms	46–60	64–77
Slice thickness, mm	5–8	5–8
Bandwidth, Hz/pixel	83.53–125	125
Slice number	12–16	12–16
NEX	1 (breathold), 4–6 (free breathing)	1 (breathhold), 10 (free breathing)
Reconstructed cardiac phase	25–30	25–30

FOV = field of view, NEX = number of excitation, TE = echo time, TR = repetition time

https://doi.org/10.3348/kjr.2020.0850

Korean Journal of Radiology
KJR

(Omniscan, General Electric Pharmaceutical Co., Ltd.) at a dose of 0.2–0.4 mL/kg body weight at a rate of 0.8–2 mL/sec. The imaging parameters are presented in Table 1. Breath holds were acquired if the patients could cooperate. Respiration of the patient who underwent sedation was not suspended during image acquisition. The acquisition times for the two sequences were recorded.

Denoising Algorithm

NLM is an algorithm used in image processing for image denoising [7,8]. A detailed description of the denoising technique is provided in the Supplement. A flowchart of the denoising process is shown in Figure 1.

Image Quality

Subjective image quality evaluation was performed by five-year and eight-year experienced radiologists based on the mid-ventricular short-axis plane of cine datasets among 2D b-SSFP and 3D b-SSSP with and without denoising. The evaluation was based on a five-point scale [9-11] (Supplement). The artifacts of cine 3D images without denoising can be seen in the Supplementary Movie 1.

The signal-to-noise ratio (SNR) of the blood pool of the left ventricle and right ventricle, septal myocardium SNR, and blood-to-myocardium contrast-to-noise ratio (CNR) were determined as objective criteria of image quality for the three sequences. Signal intensity (SI) was assessed in 20 randomly selected patients. SNRs were determined as SI blood or myocardium/SI air. The contrast between the blood and myocardium was defined as the SI blood/SI myocardium.

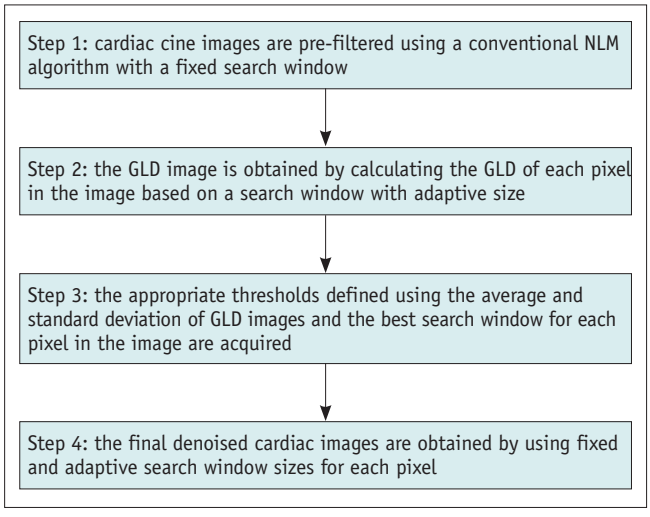

Fig. 1. Flowchart for denoising. GLD = gray level difference, NLM = non-local means

Biventricular Function Analysis

Image analysis was performed offline using commercial software (CVI42, Circle Cardiovascular Imaging Inc.). The following parameters were calculated: biventricular end-diastolic volume (EDV), end-systolic volume (ESV), stroke volume (SV) and ejection fraction (EF). Each cine 2D b-SSFP image, cine 3D b-SSFP image, and cine 3D b-SSFP image with denoising was anonymized and randomized for two radiologists (with 20 years and 25 years' experience in cardiac image diagnosis) to independently perform segmentation. To test intra-observer variability, the functional analysis was repeated by the radiologist with 20 years' experience in a subset of 10 randomly selected participants eight weeks later. Inter-observer variability was tested in the same subset of participants by the radiologist with 25 years' experience.

Statistical Analysis

All statistical analyses were performed using SPSS software (version 24.0; IBM Corp.). The mean ± standard deviation (SD) was calculated for all the parameters. Comparisons among the three groups were made using one-way analysis of variance (ANOVA) for normally distributed data and the Kruskal-Wallis test for non-normally distributed continuous variables. Pearson's correlation coefficient or Spearman's rank coefficient was used to assess the correlation between the functional parameters assessed in the three different groups. Kappa analysis was used to evaluate the consistency of image scoring by the two radiologists. A kappa value of > 0.6 represented good consistency. Intra- and inter-observer variabilities were assessed using a one-way intraclass correlation coefficient (ICC) and its 95% confidence interval (CI). Statistical significance was set at $p < 0.05$.

RESULTS

Demographics

In 35 patients, cine 2D b-SSFP and cine 3D b-SSFP were successfully performed. Two patients were sedated. Twenty-one patients were able to cooperate with breath holding. Fourteen patients underwent free breathing. No subjects were excluded because of insufficient image quality. The mean heart rate ± SD was 84.2 ± 14.7 bpm (range, 59–134 bpm). The complete demographic data are summarized in Table 2. The mean image acquisition time ± SD of cine 2D b-SSFP and cine 3D b-SSFP was 277.6 ± 0.7 seconds and

https://doi.org/10.3348/kjr.2020.0850

Table 2. Subject Characteristics

	Patients (n = 35)
Age, year	12 (7–18)
Sex, male (%)	27 (77)
BSA, m^2	1.2 (0.7–1.8)
Heart rate, bpm	84.2 (59–134)
Height, m	146.0 (79.5–176)
Weight, kg	39.1 (15–70)
Duration after surgery, year	10.3 (1–15)

Data are mean (range) unless specified otherwise. BSA = body surface area

25.1 ± 2.4 seconds, respectively. The image acquisition times of the 3D sequences were significantly shorter than those of the 2D sequences ($p < 0.001$).

Image Quality

The comparison of cine 2D b-SSFP and cine 3D b-SSFP images in different planes is shown in Figure 2. The image quality of cine 2D b-SSFP, cine 3D b-SSFP, and cine 3D b-SSFP with denoising was sufficient for contour detection in 35 patients (Figs. 3, 4). The 3D cine images had fewer respiratory registration artifacts than the 2D cine images. The mean image quality score ± SD of cine 2D b-SSFP (4.5 ± 0.5) was greater than that of cine 3D b-SSFP (3.5 ± 0.6); this difference was statistically significant ($p < 0.001$). The image quality score of 3D b-SSFP with denoising was better than that of cine 3D b-SSFP (3.8 ± 0.6 vs. 3.5 ± 0.6); this difference was also statistically significant ($p = 0.005$). The kappa value of the cine 2D b-SSFP images between the two radiologists was 0.805, while the kappa value of cine 3D b-SSFP images was 0.615 and that of cine 3D b-SSFP denoising images was 0.763.

The comparisons of SNR of the blood pool of the left ventricle and right ventricle, septal myocardium SNR, and blood-to-myocardium CNR among the three groups were significantly different ($p < 0.05$), except for septal myocardium SNR ($p > 0.05$). The SNR for blood of the left and right ventricles of cine 3D b-SSFP with denoising was more than two-fold higher than that of cine 3D b-SSFP ($p < 0.001$). The CNR of cine 3D b-SSFP with denoising was also larger than that of cine 3D b-SSFP ($p < 0.001$) (Table 3).

Biventricular Volume Quantifycation

Ventricular metrics measured using cine 2D b-SSFP, cine 3D b-SSFP, and cine 3D b-SSFP denoising imaging and correlation coefficients are shown in Tables 4, 5, and 6, respectively. The analyses of ventricular measurements for images acquired with breath hold or free breathing are shown in the Supplement (Supplementary Tables 1, 2). There were no statistically significant differences in the measurements of biventricular volumes between cine 2D b-SSFP and cine 3D b-SSFP irrespective of denoising. There was a stronger correlation ($p < 0.001$) between 3D denoising images and cine 2D b-SSFP images for quantification of biventricular measurements than cine 3D b-SSFP and cine 2D b-SSFP sequences except for left ventricular cardiac output. There were no statistically significant differences in the measurements of biventricular volumes among the three groups irrespective of breath conditions during the image acquisition process.

Intra- and Inter-Observation Agreements

The intra-observer and inter-observer ICCs are shown in Table 7. Bland-Altman plots for left ventricular and right ventricular metrics measured by the same viewer at different times and by different viewers are shown in the Supplement (Supplementary Figs. 1, 2). The largely overlapping EFs illustrate that there were no significant differences in intra- and inter-observer variability with cine 2D b-SSFP, cine 3D b-SSFP, and cine 3D b-SSFP denoising imaging, and the derived left ventricular and right ventricular metrics.

DISCUSSION

CMR is the gold standard for quantifying cardiac function [12]. Routine CMR follow-up is necessary for asymptomatic patients with rTOF, and EDV is an important parameter for guiding the optimal timing of pulmonary valve replacement [13-15]. However, it is more difficult to encourage young children to cooperate with CMR examinations because of their limited tolerance; thus, sedation and anesthesia are typically required. Barton et al. [16] revealed that early exposure to anesthesia causes permanent structural and functional changes in the central nervous system of laboratory animals. Tucker et al. [17] demonstrated a link between anesthetic exposure and negative neurodevelopmental or cognitive outcomes. McCann et al. [18] reported that exposure of just under an hour to sevoflurane-based general anesthesia in infancy does not increase the risk of adverse neurodevelopmental outcomes at two years of age. Ing et al. [19] found that there was an increase risk of language and cognitive deficit was identified in children exposed under age 3, but not in those exposed over age 3. Overall, definitive evidence of

https://doi.org/10.3348/kjr.2020.0850

Korean Journal of Radiology
KJR

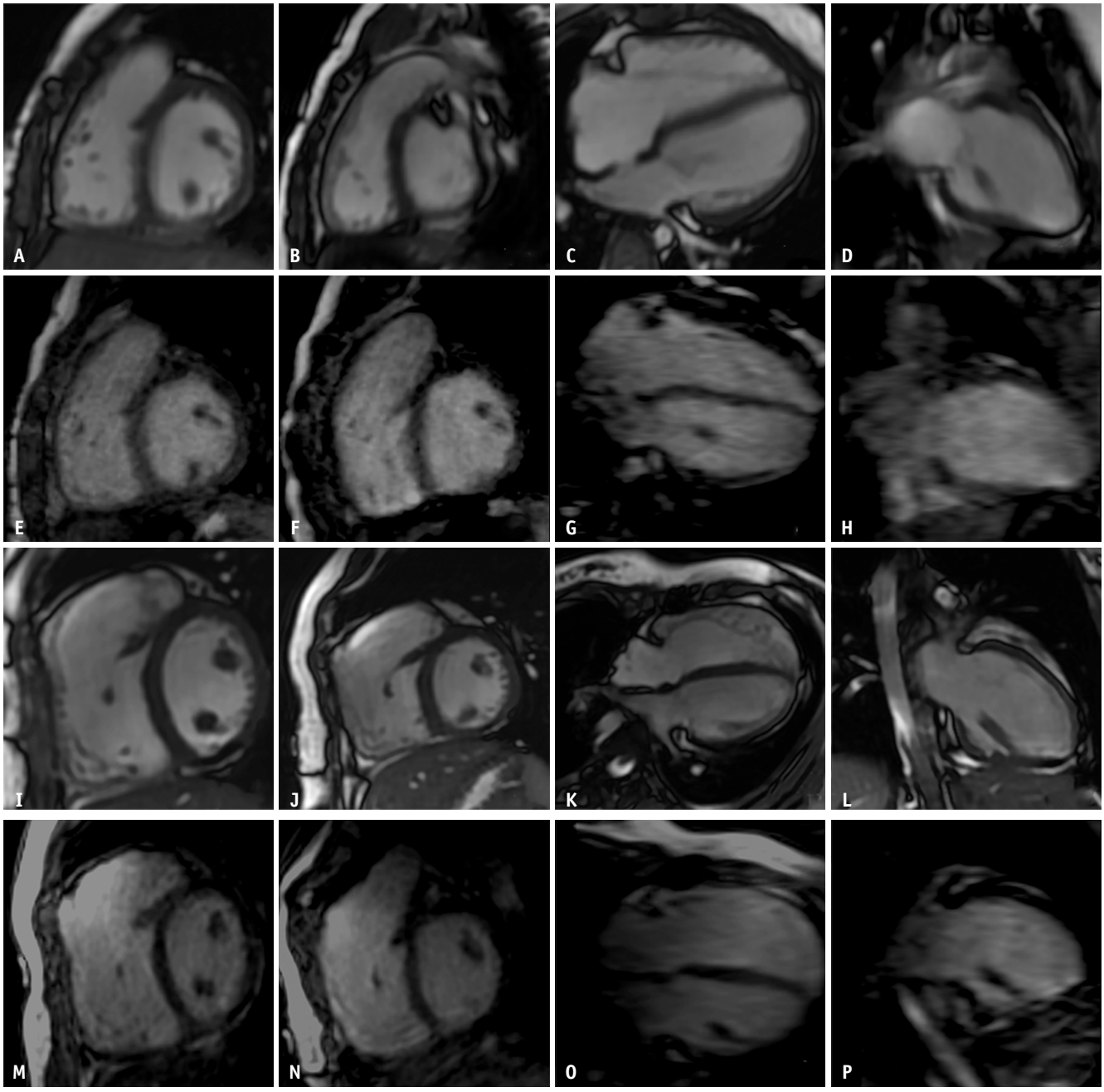

Fig. 2. Comparison of cine 2D b-SSFP and cine 3D b-SSFP images in different planes.
Figure **A-H** images acquired using 2D b-SSFP **(A-D)** and 3D b-SSFP **(E-H)** with free breathing in short axis, RVOT, 4CH, and LV 2CH respectively. Figure **I-P** images acquired using 2D b-SSFP **(I-L)** and 3D b-SSFP **(M-P)** with breath hold in short axis, RVOT, 4CH, and LV 2CH respectively. Cine 3D b-SSFP is a non-isotropic sequence; however, the RVOT orientation is similar to the short axis, such that, the image quality of the reformatted image is acceptable but will suffer in 4CH or 2CH orientations. b-SSFP = balanced steady-state free precession, D = dimensional, LV = left ventricle, RVOT = right ventricular outflow tract, 2CH = 2-chamber, 4CH = 4-chamber

toxicity was mostly found in various animal models, while anesthesia-induced neurotoxicity in the developing human brain remains unclear. One way to reduce any potential adverse effects is by reducing the time required for image acquisition. Therefore, shortening the scanning time of CMR is a consideration of researchers in the context of MRI.

To obtain data about cardiac function, several cardiac imaging planes should be performed with relatively long acquisition times using conventional cine 2D b-SSFP, which includes four-chamber, three-chamber, two-chamber, and short-axis views of both the right and left ventricles. The recently developed cine 3D b-SSFP fast image acquisition

https://doi.org/10.3348/kjr.2020.0850

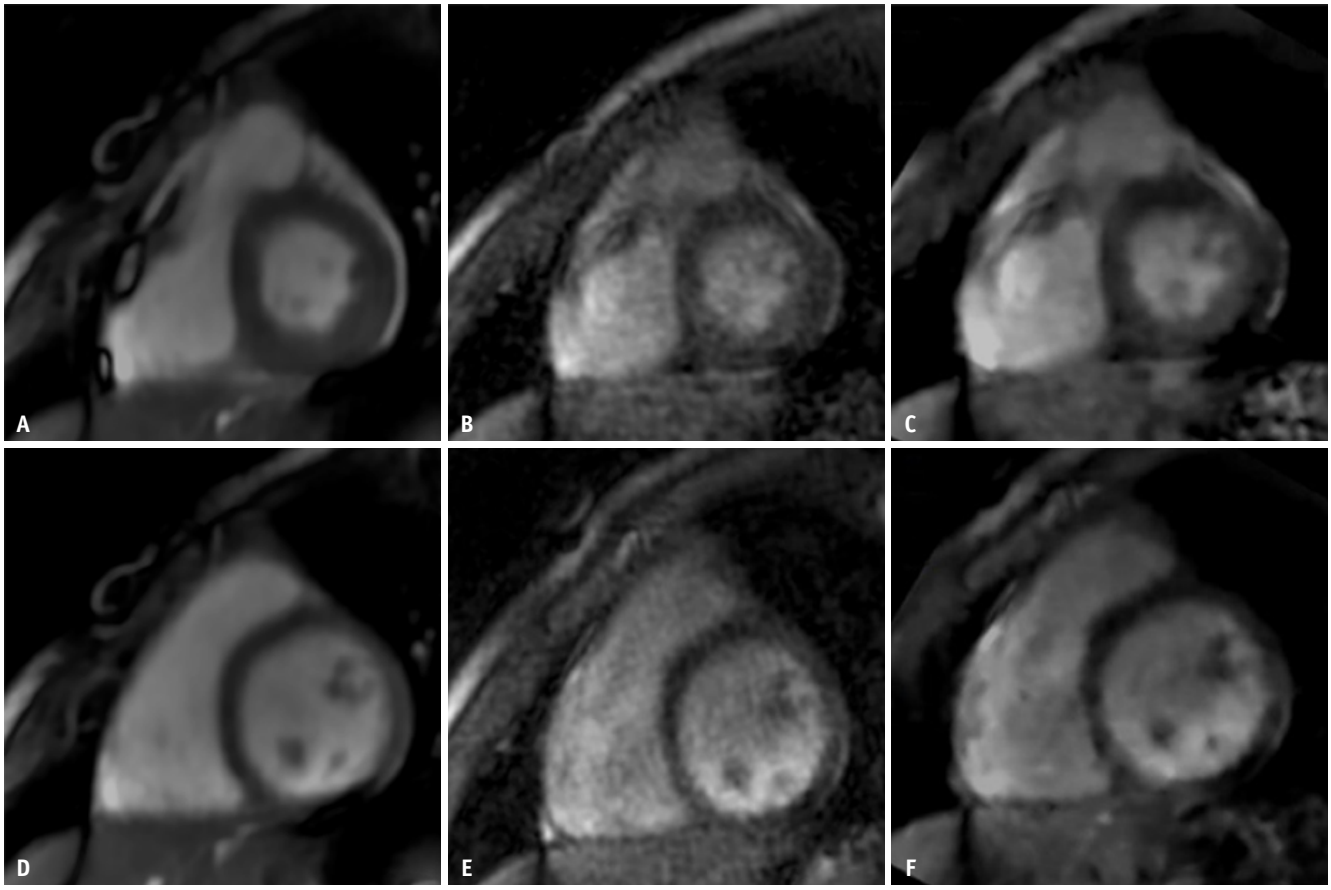

Fig. 3. A 7-year-old boy with repaired tetralogy of Fallot.
Cine cardiac magnetic resonance under free breathing scanning. Matching the mid-ventricular short-axis slice acquired using 2D b-SSFP **(A, D)**, 3D b-SSFP **(B, E)**, and 3D denoising **(C, F)**. The representative end-systolic and end-diastolic period figures are **A, B, C** and **D, E, F,** respectively. b-SSFP = balanced steady-state free precession, D = dimensional

sequence covers the entirety of ventricles and can complete the scan in a single breath hold. The acquired 3D images can be reformatted in multiple appropriate planes such as two-chamber, four-chamber, and short-axis views [5,20], and the time of image acquisition is shortened by seconds. The CNR and SNR between the 2D and 3D sequences have little difference. The main advantage of the 2D b-SSFP sequence is its relatively better SNR and CNR than the 3D b-SSFP sequence. The pitfall of 2D b-SSFP includes multiple prolonged breath holds, which increases examination time and may cause patient restlessness and slice misregistration. In addition, the 2D sequence is more sensitive to the b0 and b1 field inhomogeneity than the 3D sequence. Comparatively, for 3D b-SSFP, the time of data acquisition is significantly reduced, the misregistration between adjacent slices is eliminated, and the accuracy of ventricular volume and mass assessment is improved [3,21-23].

According to our study, the 3D images of patients with rTOF can be acquired in 25.1 ± 2.4 seconds (approximately 30 seconds) as opposed to 277.6 ± 0.7 seconds (almost 7 minutes) for 2D images. The image acquisition time of the 3D sequence was significantly shorter than that of the 2D sequence ($p < 0.05$), which is similar to the results reported by Jeong et al. [4] who used the same acquisition technique (1.5T). Jeong et al. [4] reported results using the cine 3D b-SSFP sequence and showed that it can greatly shorten the average acquisition time compared with the traditional cine 2D sequence (0.4 minutes vs. 8.5 ± 2.3 minutes; $p = 0.002$).

Respiratory and cardiac ghosts are caused by respiratory or cardiac motion occurring during imaging acquisition, especially in children. This is because heart rate and respiratory rate are comparatively faster in children than in adults, and children are often incapable of cooperating during breath hold procedures. Compared with short-axis cine 2D b-SSFP images, the reformatted cine 3D b-SSFP images, irrespective of denoising, had worse subjective and objective image quality scores. Despite this, our study

https://doi.org/10.3348/kjr.2020.0850

Korean Journal of Radiology
KJR

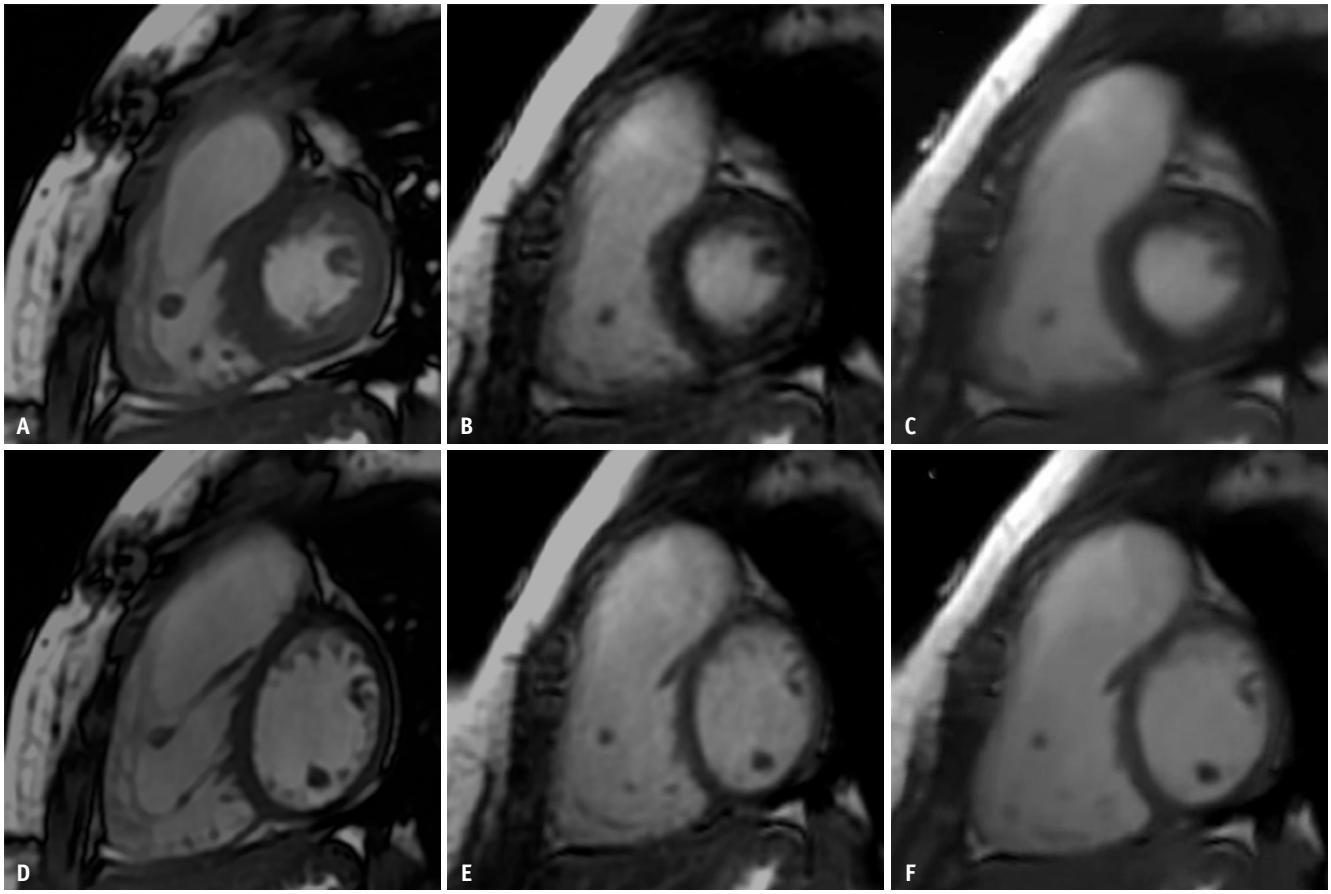

Fig. 4. A 15-year-old girl with repaired tetralogy of Fallot.
Cine cardiac magnetic resonance under breath hold scanning. Matching the mid-ventricular short-axis slice acquired using 2D b-SSFP **(A, D)**, 3D b-SSFP **(B, E)**, and 3D denoising **(C, F)**. The representative end-systolic and end-diastolic period figures are **A, B, C** and **D, E, F,** respectively.
b-SSFP = balanced steady-state free precession, D = dimensional

demonstrated that the image quality of cine 3D b-SSFP with or without denoising is feasible for use in improving diagnosis and analysis in the clinical setting. There was good consistency in image quality scoring among the three methods between the two radiologists.

Cine 3D MRI demonstrates slight blurring, some loss of signals, and reduced intensity contrast; the blurring and loss of signals are likely to be a result of acceleration [22]. For kat ARC, Lai et al. [24,25] reported that k-space data were acquired with time-shifted sampling, and missing k-space data were recovered using a k-t synthesis kernel with a temporal window selection adapted to the local cardiac motion at each cardiac phase. The reduced intensity contrast was due to volumetric acquisition, signal saturation in the cardiac blood pool, and shorter repetition time [26-28]. Several strategies can be used to optimize the sequence and improve image quality. Previous studies have shown that variable flip angle cine 3D b-SSFP using k-space acquisition, which is not synchronized with the cardiac cycle, produced higher contrast in cardiac imaging [29]. Another study demonstrated that a lack of intrinsic contrast can be overcome using a T1 shortening agent [30]. Myocardial blood pool contrast could be improved by injecting a contrast agent (cine 3D b-SSFP was performed after contrast agent injection). Other studies have revealed that the 32-channel dedicated cardiac phased array coil can simultaneously improve the SNR and image acquisition efficiency of 3D images [15,16]. Noise in MRI reduces image contrast; hence, the denoising technique can improve image contrast [6,20]. Therefore, at our center, three strategies were used: adjustment of the flip angle (small flip angle), post-contrast injection scanning, and image denoising techniques.

To overcome the deficiencies of so-called acquisition-based noise reduction, increasing the acquisition time or decreasing the spatial resolution through post-processing noise reduction methods were proposed. Image denoising preserves important features (e.g., the original edges and

https://doi.org/10.3348/kjr.2020.0850

Table 3. Signal-to Noise and BM Contrast-to-Noise

Parameter	2D b-SSFP	3D b-SSFP	3D b-SSFP Denoised	*P*		
				2D b-SSFP vs. 3D b-SSFP	2D b-SSFP vs. 3D b-SSFP Denoised	3D b-SSFP vs. 3D b-SSFP Denoised
LV SNR	127.1 ± 33.4	120.6 ± 61.6	297.2 ± 120.4	0.003	< 0.001	< 0.001
RV SNR	130.2 ± 33.7	135.2 ± 77.6	316.3 ± 119.5	0.004	< 0.001	< 0.001
SM SNR	40.4 ± 11.6	50.3 ± 22.3	140.7 ± 75.2	0.435	0.998	0.400
BM CNR	3.3 ± 0.5	2.5 ± 0.5	2.3 ± 0.5	< 0.001	0.030	< 0.001

Data are mean ± standard deviation. b-SSFP = balanced steady-state free precession, BM = blood-to myocardium, CNR = contrast-to-noise ratio, D = dimensional, LV = left ventricular, RV = right ventricular, SM = septal myocardium, SNR = signal-to-noise ratio

Table 4. Ventricular Metrics Measured Using Cine 2D b-SSFP, Cine 3D b-SSFP and Cine 3D b-SSFP Denoising Imaging

Parameters	2D b-SSFP	3D b-SSFP	3D b-SSFP Denoised	*P*		
				2D b-SSFP vs. 3D b-SSFP	2D b-SSFP vs. 3D b-SSFP Denoised	3D b-SSFP vs. 3D b-SSFP Denoised
EDV, mL						
LV	97.8 ± 24.8	100.4 ± 25.3	100.1 ± 25.6	0.662	0.704	0.955
RV	159.4 ± 64.5	153.6 ± 61.7	155.4 ± 66.3	0.708	0.795	0.908
ESV, mL						
LV	42.7 ± 12.9	44.0 ± 13.3	44.3 ± 13.2	0.690	0.621	0.923
RV	85.0 ± 40.3	87.1 ± 42.0	84.7 ± 43.0	0.839	0.972	0.812
SV, mL						
LV	55.1 ± 14.8	56.4 ± 14.2	55.5 ± 15.1	0.710	0.908	0.797
RV	74.4 ± 31.4	69.4 ± 24.4	70.7 ± 29.0	0.468	0.593	0.849
EF, %						
LV	56.5 ± 6.6	56.3 ± 5.3	56.1 ± 6.7	0.903	0.786	0.881
RV	47.8 ± 10.5	45.8 ± 7.3	47.2 ± 9.7	0.369	0.789	0.527

Data are mean ± standard deviation. b-SSFP = balanced steady-state free precession, D = dimensional, EDV = end-diastolic volume, EF = ejection fraction, ESV = end-systolic volume, LV = left ventricular, RV = right ventricular, SV = stroke volume

Table 5. Ventricular Metrics Measured Using Cine 2D b-SSFP, Cine 3D b-SSFP and Cine 3D b-SSFP Denoising Imaging, Indexed for Body Surface Area

Parameters	2D b-SSFP	3D b-SSFP	3D b-SSFP Denoised
EDV, mL/m^2			
LV	79.5 ± 10.2	81.2 ± 9.6	81.4 ± 9.8
RV	128.8 ± 41.1	125.1 ± 40.6	125.2 ± 27.5
ESV, mL/m^2			
LV	34.5 ± 6.5	35.7 ± 6.3	35.5 ± 6.1
RV	69.2 ± 29.9	67.6 ± 29.8	69.9 ± 27.5
SV, mL/m^2			
LV	45.0 ± 7.4	45.3 ± 7.5	46.0 ± 6.4
RV	60.4 ± 19.7	57.5 ± 17.9	57.5 ± 19.1
EF, %/m^2			
LV	49.2 ± 15.8	48.8 ± 15.8	48.9 ± 15.4
RV	41.4 ± 15.2	41.4 ± 16.4	40.3 ± 15.14

Data are mean ± standard deviation. b-SSFP = balanced steady-state free precession, D = dimensional, EDV = end-diastolic volume, EF = ejection fraction, ESV = end-systolic volume, LV = left ventricular, RV = right ventricular, SV = stroke volume

Table 6. Comparison of Correlations between Cine 2D b-SSFP, Cine 3D b-SSFP and Cine 3D b-SSFP Denoising Imaging in Cardiac Function of Repaired Tetralogy of Fallot

Parameters	2D b-SSFP vs. 3D b-SSFP		2D b-SSFP vs. 3D b-SSFP Denoised	
	r	*P*	*r*	*P*
EDV, mL/m^2				
LV	0.980	< 0.001	0.991	< 0.001
RV	0.948	< 0.001	0.965	< 0.001
ESV, mL/m^2				
LV	0.937	< 0.001	0.979	< 0.001
RV	0.922	< 0.001	0.936	< 0.001
SV, mL/m^2				
LV	0.943	< 0.001	0.975	< 0.001
RV	0.821	< 0.001	0.829	< 0.001
EF, %/m^2				
LV	0.853	< 0.001	0.959	< 0.001
RV	0.256	0.137	0.758	< 0.001

b-SSFP = balanced steady-state free precession, D = dimensional, EDV = end-diastolic volume, EF = ejection fraction, ESV = end-systolic volume, LV = left ventricular, RV = right ventricular, SV = stroke volume

https://doi.org/10.3348/kjr.2020.0850

Korean Journal of Radiology
KJR

Table 7. Intra-Observer and Inter-Observer Variability

Parameters	2D b-SSFP		3D b-SSFP		3D b-SSFP Denoised	
	Intra-Observer	Inter-Observer	Intra-Observer	Inter-Observer	Intra-Observer	Inter-Observer
LV EDV	0.991 (0.963, 0.998)	0.998 (0.994, 1.000)	0.980 (0.921, 0.995)	0.990 (0.959, 0.997)	0.998 (0.990, 0.999)	0.999 (0.994, 1.000)
LV ESV	0.995 (0.982, 0.999)	0.995 (0.908, 0.999)	0.937 (0.770, 0.984)	0.968 (0.870, 0.992)	0.974 (0.907, 0.994)	0.993 (0.973, 0.998)
LV SV	0.995 (0.981, 0.999)	0.999 (0.997, 1.000)	0.984 (0.935, 0.996)	0.992 (0.967, 0.998)	0.913 (0.690, 0.978)	0.981 (0.924, 0.995)
LV EF	0.958 (0.841, 0.989)	0.974 (0.894, 1.000)	0.660 (0.096, 0.903)	0.795 (0.176, 0.949)	0.938 (0.772, 0.984)	0.899 (0.594, 0.975)
RV EDV	1.000 (0.999, 1.000)	0.999 (0.995, 1.000)	0.993 (0.971, 0.998)	0.996 (0.985, 0.999)	1.000 (0.999, 1.000)	1.000 (0.999, 1.000)
RV ESV	0.999 (0.994, 1.000)	0.999 (0.993, 1.000)	0.985 (0.941, 0.996)	0.992 (0.969, 0.998)	0.999 (0.995, 1.000)	1.000 (0.999, 1.000)
RV SV	1.000 (0.999, 1.000)	0.999 (0.994, 1.000)	0.880 (0.592, 0.969)	0.936 (0.743, 0.984)	0.998 (0.994, 1.000)	0.998 (0.990, 0.999)
RV EF	0.997 (0.988, 0.999)	0.993 (0.973, 0.998)	0.681 (0.134, 0.910)	0.810 (0.236, 0.953)	0.979 (0.919, 0.995)	0.987 (0.947, 0.997)

Data are intraclass correlation coefficient values with their 95% confidence interval in parentheses. b-SSFP = balanced steady-state free precession, D = dimensional, EDV = end-diastolic volume, EF = ejection fraction, ESV = end-systolic volume, LV = left ventricular, RV = right ventricular, SV = stroke volume

texture of the image) while removing image noise. Many image denoising methods have been explored, including approaches based on anisotropic diffusion filters, the NLM algorithm, and the wavelet transform. NLM filters have been used for feature-preserved MRI denoising [31,32]. NLM algorithms with an adaptive isotropic search window size are used to increase the adaptive isotropic search window size based on the traditional NLM algorithm, which can avoid denoising performance degradation as noise variance increases. This method effectively preserves image details (e.g., edges and textures) at higher noise levels. One study demonstrated that denoising methods, such as convolutional neural network-based methods, have shown promising results in computed tomography [33]. In our study, images acquired using the cine 3D b-SSFP sequence had motion artifacts and low contrast between the myocardium and the blood pool. Therefore, the NLM algorithm with an adaptive isotropic search window size was used to denoise the cardiac image, preserve the ventricular contour, and increase the contrast between the myocardium and the blood pool.

Accurate measurement of ventricular volume is paramount from a clinical point of view. The 3D image data from computed tomography or MRI may provide highly accurate and reproducible ventricular and SVs [34]. In our study, the functional parameters of the three groups were not significantly different ($p > 0.05$). Cardiac function data obtained using cine 3D b-SSFP with denoising were more similar to those obtained using cine 2D imaging because cine 3D b-SSFP with denoising demonstrated a higher signal and contrast between the blood and the myocardium. According to the breath holding and free breathing subgroups, the biventricular functional measurements of the three different groups showed no significant statistical differences ($p > 0.05$), which excluded the influence of breath on acquiring accurate ventricular function.

Correlation analysis of biventricular EDV, ESV, SV, and EF in cine 2D b-SSFP vs. cine 3D b-SSFP with or without denoising was performed in our group. Cine 3D b-SSFP with denoising vs. cine 2D b-SSFP had a better correlation coefficient than cine 3D b-SSFP vs. cine 2D b-SSFP for EDV, ESV, SV, and EF of the left (0.959–0.991; $p < 0.001$), as well as right ventricular (0.755–0.965; $p < 0.001$) metrics. The correlation coefficients (0.853–0.980) for the four left ventricular measurements with cine 3D b-SSFP vs. cine 2D b-SSFP were significant ($p < 0.001$ for all).

For the cine 2D b-SSFP sequence, the ICC was similar to

https://doi.org/10.3348/kjr.2020.0850

previously published data [24], with right ventricular data having greater variability compared with left ventricular data. This was expected because of the greater difficulty in segmenting the more trabeculated and complex-shaped right ventricle. Importantly, the intra-observer and inter-observer variabilities of cine 3D b-SSFP with or without denoising were similar to those observed with cine 2D b-SSFP. This is an important finding, as demonstrating reliability is vital for clinical translation. With regards to the Bland-Altman analysis, our results using cine 3D b-SSFP with denoising revealed less statistical variance in the parameters assessed in the biventricular analysis compared with cine 3D b-SSFP, except for left ventricular SV in intra- and inter-observer variability.

The present study has several limitations. First, the acquisition time of cine 3D b-SSFP was not short enough (average 25 seconds) because it was challenging to encourage children to complete image acquisition in a breath hold. Second, the sample size was limited. The number of children of different ages and genders was unevenly distributed. It was impossible to conduct a stratified analysis on all age groups, and gender stratification analysis could not be conducted. The sample size should be increased in future studies.

In conclusion, the 3D b-SSFP sequence can significantly reduce acquisition time compared to the 2D b-SSFP sequence for cine imaging in the evaluation of ventricular function in children with rTOF, and its quality can be further improved by combining it with an NLM denoising method.

Supplement

The Supplement is available with this article at https://doi.org/10.3348/kjr.2020.0850.

Supplementary Movie Legend

Movie 1. Patent 1: a 7-year-old boy with rTOF. Artifacts of cine 3D b-SSFP CMR under free breathing scanning. Patient 2: a 15-year-old girl with rTOF. Artifacts of cine 3D b-SSFP CMR under breath hold scanning.

Conflicts of Interest

The authors have no potential conflicts of interest to disclose.

Author Contributions

Conceptualization: YaFeng Peng, LiWei Hu, YuMin Zhong. Data curation: YaFeng Peng. Formal analysis: YaFeng Peng. Funding acquisition: YuMin Zhong. Investigation: YaFeng Peng, XinYu Su, LiWei Hu, Qian Wang, RongZhen Ouyang, AiMin Sun, Chen Guo. Methodology: LiWei Hu, YuMin Zhong, Yong Zhang, LiJia Wang. Project administration: YuMin Zhong. Resources: YuMin Zhong. Software: XinYu Su, LiJia Wang, YuMin Zhong. Supervision: YuMin Zhong. Validation: RongZhen Ouyang, LiWei Hu, XiaoFen Yao. Visualization: YaFeng Peng. Writing—original draft: YaFeng Peng, YuMin Zhong. Writing—review & editing: YaFeng Peng, YuMin Zhong.

ORCID iDs

YaFeng Peng
https://orcid.org/0000-0001-7381-4695
XinYu Su
https://orcid.org/0000-0002-4993-458X
LiWei Hu
https://orcid.org/0000-0003-2710-9957
Qian Wang
https://orcid.org/0000-0002-9438-0723
RongZhen Ouyang
https://orcid.org/0000-0002-9614-3692
AiMin Sun
https://orcid.org/0000-0002-9235-8960
Chen Guo
https://orcid.org/0000-0003-1190-2061
XiaoFen Yao
https://orcid.org/0000-0003-1182-2109
Yong Zhang
https://orcid.org/0000-0002-9887-5125
LiJia Wang
https://orcid.org/0000-0002-8175-7720
YuMin Zhong
https://orcid.org/0000-0002-0164-8752

REFERENCES

1. Fratz S, Chung T, Greil GF, Samyn MM, Taylor AM, Valsangiacomo Buechel ER, et al. Guidelines and protocols for cardiovascular magnetic resonance in children and adults with congenital heart disease: SCMR expert consensus group on congenital heart disease. *J Cardiovasc Magn Reson* 2013;15:51
2. Kramer CM, Barkhausen J, Flamm SD, Kim RJ, Nagel E. Standardized cardiovascular magnetic resonance (CMR) protocols 2013 update. *J Cardiovasc Magn Reson* 2013;15:91

3. Maffei E, Messalli G, Martini C, Rossi A, van Pelt N, van Geuns RJ, et al. Magnetic resonance assessment of left ventricular volumes and mass using a single-breath-hold 3D k-t BLAST cine b-SSFP in comparison with multiple-breath-hold 2D cine b-SSFP. *Insights Imaging* 2011;2:39-45
4. Jeong D, Schiebler ML, Lai P, Wang K, Vigen KK, François CJ. Single breath hold 3D cardiac cine MRI using kat-ARC: preliminary results at 1.5T. *Int J Cardiovasc Imaging* 2015;31:851-857
5. Moghari MH, Barthur A, Amaral ME, Geva T, Powell AJ. Free-breathing whole-heart 3D cine magnetic resonance imaging with prospective respiratory motion compensation. *Magn Reson Med* 2018;80:181-189
6. Anand CS, Sahambi JS. Wavelet domain non-linear filtering for MRI denoising. *Magn Reson Imaging* 2010;28:842-861
7. Buades A, Coll B, Morel J. A review of image denoising algorithms, with a new one. *Multiscale Model Simul* 2005;4:490-530
8. Verma R, Pandey R. Non local means algorithm with adaptive isotropic search window size for image denoising. Proceedings of 2015 Annual IEEE India Conference (INDICON); 2015 Dec 17-20; New Delhi, India: IEEE; 2015; p. 1-5
9. Feng L, Srichai MB, Lim RP, Harrison A, King W, Adluru G, et al. Highly accelerated real-time cardiac cine MRI using k-t SPARSE-SENSE. *Magn Reson Med* 2013;70:64-74
10. Haji-Valizadeh H, Rahsepar AA, Collins JD, Bassett E, Isakova T, Block T, et al. Validation of highly accelerated real-time cardiac cine MRI with radial k-space sampling and compressed sensing in patients at 1.5T and 3T. *Magn Reson Med* 2018;79:2745-2751
11. Matsumoto H, Matsuda T, Miyamoto K, Nakatsuma K, Sugahara M, Shimada T. Feasibility of free-breathing late gadolinium-enhanced cardiovascular MRI for assessment of myocardial infarction: navigator-gated versus single-shot imaging. *Int J Cardiol* 2013;168:94-99
12. Qi H, Bustin A, Cruz G, Jaubert O, Chen H, Botnar RM, et al. Free-running simultaneous myocardial T1/T2 mapping and cine imaging with 3D whole-heart coverage and isotropic spatial resolution. *Magn Reson Imaging* 2019;63:159-169
13. de Torres-Alba F, Kaleschke G, Baumgartner H. Impact of percutaneous pulmonary valve implantation on the timing of reintervention for right ventricular outflow tract dysfunction. *Rev Esp Cardiol (Engl Ed)* 2018;71:838-846
14. Tatewaki H, Shiose A. Pulmonary valve replacement after repaired tetralogy of Fallot. *Gen Thorac Cardiovasc Surg* 2018;66:509-515
15. Tweddell JS, Simpson P, Li SH, Dunham-Ingle J, Bartz PJ, Earing MG, et al. Timing and technique of pulmonary valve replacement in the patient with tetralogy of Fallot. *Semin Thorac Cardiovasc Surg Pediatr Card Surg Annu* 2012;15:27-33
16. Barton K, Nickerson JP, Higgins T, Williams RK. Pediatric anesthesia and neurotoxicity: what the radiologist needs to know. *Pediatr Radiol* 2018;48:31-36
17. Tucker EW, Jain SK, Mahesh M. Balancing the risks of radiation and anesthesia in pediatric patients. *J Am Coll Radiol* 2017;14:1459-1461
18. McCann ME, de Graaff JC, Dorris L, Disma N, Withington D, Bell G, et al. Neurodevelopmental outcome at 5 years of age after general anaesthesia or awake-regional anaesthesia in infancy (GAS): an international, multicentre, randomised, controlled equivalence trial. *Lancet* 2019;393:664-677
19. Ing CH, DiMaggio CJ, Whitehouse AJ, Hegarty MK, Sun M, von Ungern-Sternberg BS, et al. Neurodevelopmental outcomes after initial childhood anesthetic exposure between ages 3 and 10 years. *J Neurosurg Anesthesiol* 2014;26:377-386
20. Menchón-Lara RM, Simmross-Wattenberg F, Casaseca-de-la-Higuera P, Martín-Fernández M, Alberola-López C. Reconstruction techniques for cardiac cine MRI. *Insights Imaging* 2019;10:100
21. Jung BA, Hennig J, Scheffler K. Single-breathhold 3D-trueFISP cine cardiac imaging. *Magn Reson Med* 2002;48:921-925
22. Greil GF, Germann S, Kozerke S, Baltes C, Tsao J, Urschitz MS, et al. Assessment of left ventricular volumes and mass with fast 3D cine steady-state free precession k-t space broad-use linear acquisition speed-up technique (k-t BLAST). *J Magn Reson Imaging* 2008;27:510-515
23. Thiele H, Nagel E, Paetsch I, Schnackenburg B, Bornstedt A, Kouwenhoven M, et al. Functional cardiac MR imaging with steady-state free precession (SSFP) significantly improves endocardial border delineation without contrast agents. *J Magn Reson Imaging* 2001;14:362-367
24. Lai P, Brau AC, Beatty PJ, Shankaranarayanan A. Highly-accelerated cardiac cine MR imaging using kats ARC (autocalibrating reconstruction for Cartesian sampling with k- & adaptive-t-space data synthesis). *Proc Intl Soc Mag Reson Med* 2009;17:767
25. Lai P, Alley MT, Vasanawala SS, Brau AC. Single-breathhold three-dimensional cardiac cine MRI with retrospective cardiac gating using high acceleration kat ARC (k- & adaptive t-autocalibrating reconstruction for Cartesian sampling). *Proc Intl Soc Mag Reson Med* 2011;19:3378
26. Holst K, Ugander M, Sigfridsson A. Left ventricular volume measurements with free breathing respiratory self-gated 3-dimensional golden angle radial whole-heart cine imaging - Feasibility and reproducibility. *Magn Reson Imaging* 2017;43:48-55
27. Amano Y, Suzuki Y, van Cauteren M. Evaluation of global cardiac functional parameters using single-breath-hold three-dimensional cine steady-state free precession MR imaging with two types of speed-up techniques: comparison with two-dimensional cine imaging. *Comput Med Imaging Graph* 2008;32:61-66
28. Makowski MR, Wiethoff AJ, Jansen CH, Uribe S, Parish V, Schuster A, et al. Single breath-hold assessment of cardiac function using an accelerated 3D single breath-hold acquisition technique--comparison of an intravascular and extravascular contrast agent. *J Cardiovasc Magn Reson* 2012;14:53

 https://doi.org/10.3348/kjr.2020.0850

29. Srinivasan S, Ennis DB. Variable flip angle balanced steady-state free precession for lower SAR or higher contrast cardiac cine imaging. *Magn Reson Med* 2014;71:1035-1043
30. van der Ven JPG, Sadighy Z, Valsangiacomo Buechel ER, Sarikouch S, Robbers-Visser D, Kellenberger CJ, et al. Multicentre reference values for cardiac magnetic resonance imaging derived ventricular size and function for children aged 0-18 years. *Eur Heart J Cardiovasc Imaging* 2020;21:102-113
31. Chen G, Zhang P, Wu Y, Shen D, Yap PT. Denoising magnetic resonance images using collaborative non-local means. *Neurocomputing* 2016;177:215-227
32. Yu H, Ding M, Zhang X. Laplacian eigenmaps network-based nonlocal means method for MR image denoising. *Sensors (Basel)* 2019;19:2918
33. Kim B, Han M, Shim H, Baek J. A performance comparison of convolutional neural network-based image denoising methods: the effect of loss functions on low-dose CT images. *Med Phys* 2019;46:3906-3923
34. Goo HW. Semiautomatic three-dimensional threshold-based cardiac computed tomography ventricular volumetry in repaired tetralogy of Fallot: comparison with cardiac magnetic resonance imaging. *Korean J Radiol* 2019;20:102-113

https://doi.org/10.3348/kjr.2020.0850